An experimental investigation of hydrodynamic cavitation in micro-Venturis

Cite as: Phys. Fluids **18**, 103603 (2006); https://doi.org/10.1063/1.2360996
Submitted: 08 April 2005 . Accepted: 12 September 2006 . Published Online: 16 October 2006

Chandan Mishra, and Yoav Peles

An experimental investigation of hydrodynamic cavitation in micro-Venturis

Chandan Mishra
Intel Corporation, Santa Clara, California 95054

Yoav Peles[a)]
Department of Mechanical, Aerospace and Nuclear Engineering, Rensselaer Polytechnic Institute, Troy, New York 12180

(Received 8 April 2005; accepted 12 September 2006; published online 16 October 2006)

The existence of hydrodynamic cavitation in the flow of de-ionized water through micro-Venturis has been witnessed in the form of traveling bubble cavitation and fully developed streamer bubble/supercavitation, and their mechanisms have been discussed. High-speed photography and flow visualization disclose inchoate cavitation bubbles emerging downstream from the micro-Venturi throat and the presence of a single streamer bubble/supercavity, which is equidistant from the micro device walls. The supercavity initiates inside the diffuser section and extends until the microchannel exit and proceeds to bifurcate the incoming flow. This article strives to provide numerical data and experimental details of hydrodynamic cavitation taking place within micro-Venturis. © *2006 American Institute of Physics*. [DOI: 10.1063/1.2360996]

I. INTRODUCTION

High-speed microfluidic systems in the form of power microelectromechanical systems devices,[1] microrockets and micropropulsion systems, micropumps, microturbomachinery, etc., have been developed in recent times following the expeditious advancement of microfabrication technology. Amid other results, microscale fluid flow studies have revealed anomalous behavior and recorded unexpected deviations from macroscale results.[2–4] Recently, the presence of hydrodynamic cavitation, the explosive growth and cataclysmic collapse of vapor bubbles, has been identified in flow through elementary micro-orifices.[5–7] The study reported several deviations from comparable conventional scale experiments and concluded that cavitation will develop in microsystems if apposite hydrodynamic conditions prevail. Pennathur *et al.*[8] indicated a rapid transition from incipient to a large attached supercavity in their work which was later observed in cavitation studies on micro-orifices.[5] However, comparable cavitation studies on micro-Venturis, which are often encountered in microfluidic devices, and concomitant scaling effects have not been investigated. Previous studies have indicated the growing importance of surface nuclei upon the shrinkage in the size of the prototype.[9] Predicting and explaining cavitation in microdevices can be challenging since a single bubble can choke the entire microchannel and alter flow conditions. In addition, the balance in the nuclei population (surface and stream), which are potential nucleation sites that promote cavitation events, will be affected by the diminutive size, growing surface tension effects, and filtered working liquids employed in microfluidic systems. Additionally, factors such as residence time for nuclei growth,[5,10] flow regimes, Weber number, Capillary number, Reynolds number, relative size of the nuclei to the paragon,[10] unique microscale cavitating flow patterns,[12] surface/material interactions,[11] etc., will play a vital role in shaping cavitation inside microfluidic systems. Therefore, flow visualization of cavitation, and the identification of assorted cavitating patterns in micro-Venturis is definitely warranted.

II. CAVITATION DEVELOPMENT IN VENTURIS AND DEFINITIONS

Venturis offer a platform for demonstrating the pernicious effects of hydrodynamic cavitation, and the flow of liquids through a Venturi element provides an ideal situation where the submicron nuclei can grow in the low-pressure region formed at the throat and collapse once the pressure recovers downstream of the constriction element in the diffuser. In addition, the hydrodynamically developing flow in the Venturi throat can force/induce sharper pressure gradients.[12] If the static pressure at the throat reaches a critical value, this hot-spot becomes a site for the rupture of the liquid and consequent growth of cavitation nuclei in the form of vapor- and gas-filled bubble/bubble clouds. The magnitude and intensity of cavitation in flow via Venturis has often been described by a classical nondimensional parameter[5,12–14] called the cavitation number (σ_V) and is defined as

$$\sigma_V = \frac{P_2 - P_v}{\frac{1}{2}\rho V_{\text{th}}^2}, \tag{1}$$

where P_2 is the exit pressure, which causes cavitation. $V_{\text{th}} = Q/A_{\text{th}}$, is the average velocity encountered at the orifice throat, while P_v is the vapor pressure of water. A_{th} is the micro-Venturi throat area. ρ is the density of the incompressible fluid (water).

III. MICROFABRICATION AND EXPERIMENTS

The micro-Venturi system tested in the current experiments is micromachined on a silicon wafer and sealed with a

[a)]Author to whom correspondence should be addressed. Telephone: 518-276-2886. Fax: 518-276-2623. Electronic mail: pelesy@rpi.edu

TABLE I. Device description and cavitation data. Note: d_h, D_h, w_V, w_C, l, and h are the micro-Venturi hydraulic diameter, microchannel hydraulic diameter, micro-orifice width, microchannel width, height of the microchannel/micro-orifice, and the length of the micro-orifice, respectively, while $\sigma_{V,i}$ and $\sigma_{V,d}$ are the average of the experimentally determined values of the incipient and desinent cavitation, respectively.

Device specifications (μm)	$C_C=\frac{A_{th}}{A_1}$	$C_E=\frac{A_{th}}{A_2}$	d_h (μm)	D_h (μm)	$\sigma_{V,i}$	$\sigma_{V,d}$
$w_V=21$ $w_C=201$ $h=101$ $l=1632$	0.1	0.1	34.77	134.44	~2.51	~3.22

Pyrex wafer through apposite bonding techniques.[5] The inlet corners are well rounded to eliminate any sharp edges while the exit diffuser angle is small (around 4°), which ensures that the flow does not separate. The micro-Venturi flow Reynolds number is defined as

$$\mathrm{Re}_h = \frac{\rho V_{th} d_h}{\mu}, \tag{2}$$

where μ is the dynamic viscosity of the incompressible fluid (water), while $d_h=4A_{th}/p$ is the hydraulic diameter of the micro-orifice and p is the perimeter of the Venturi throat cross section (rectangular). The maximum micro-Venturi throat Reynolds numbers ($\mathrm{Re}_{h,\max}\simeq 750$) encountered in the current exercise is firmly entrenched in the laminar regime. The microfluidic device is equipped with pressure ports taps, which are positioned at upstream and downstream of the micro-Venturi to facilitate *in situ* measurements of the static pressures inside the microfluidic device. Essential device dimensions are measured and listed in Table I.

De-ionized water is the working fluid for all experiments, and the liquid is delivered from the inlet container through a calibrated flow meter. The flow rate is manipulated by the pressure differential across the micro-Venturi, which is achieved by controlling the pressure of the inlet and the exit chambers. Pressure and flow rate data are collected for different exit pressures via the LABVIEW® interface. Under suitable hydrodynamic conditions, cavitation events commence and images of cavitating flow patterns are recorded. The dissolved oxygen concentration is continuously monitored and randomly measured in between the experiments and is estimated to be 8.7 ± 1 ppm. The liquid is not recirculated but discarded once the exit chamber is filled up. The mean uncertainties[15] linked with the measurement of pressure, liquid volumetric flow rate, and the cavitation index, are 0.25%, 1%, and 7%–8%, respectively. Flow visualization of various cavitation flow patterns and images of cavitation bubbles is captured by a Phantom v4.2 SR-CMOS sensor-based high-speed camera.

IV. RESULTS AND DISCUSSION

A. Flow visualization

Assorted cavitating flow patterns are observed as the flow rate is increased through a reduction of the exit pressure, for a fixed inlet pressure. At first tiny incipient bubbles (traveling bubble/inception, $\sigma_{V,i}$) are sighted immediately downstream of the micro-Venturi throat [Fig. 1(a)] at high velocities quite unlike past macroscale Venturi experiments,[9,14,16] which reported that traveling bubble cavitation occurs consistently at/inside the Venturi throat.[13,14,17,18] The bubbles collapse a few hydraulic diameters downstream of the Venturi exit; i.e., either in the diffuser or inside the microchannel. At times these bubbles have been spotted growing on the microdevice surface and collapsing after being dragged downstream by the incoming high-velocity flow.

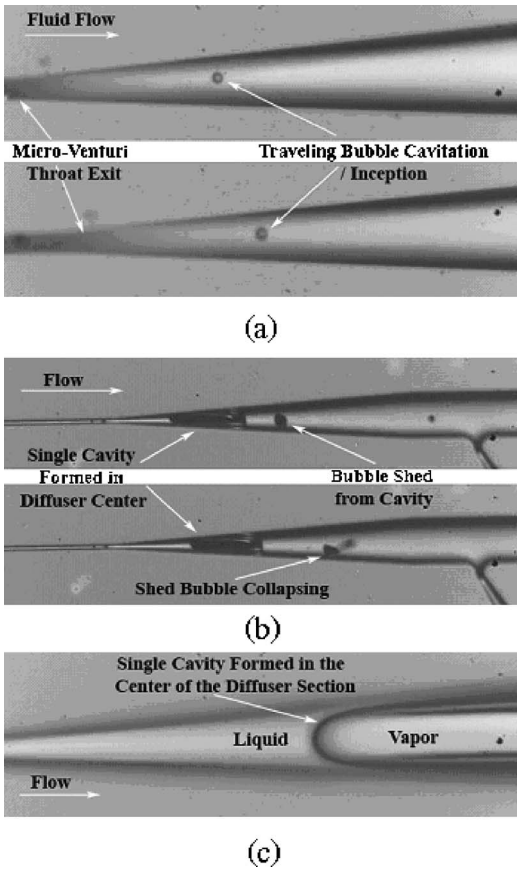

FIG. 1. (a) Traveling bubble cavitation/cavitation Inception ($\sigma_{V,i}=2.46$). (b) Development of vapor cavity in the diffuser region ($\sigma_V=2.32$). (c) Close-in image of the vapor cavity showing its location in the center of the diffuser section.

A marginal change in the cavitation number, beyond the first appearance of traveling bubble cavitation, results in the formation of a small cavity immediately ($4d_h-5d_h$) downstream of the micro-Venturi throat [Fig. 1(b)]. The unsteady cavity is located right in the middle of the diffuser boundaries and the liquid flows on both sides of the cavity encompassing it. Tiny bubbles are shed from the cavity and at times the entire cavity is dragged away by the flow. Transition from traveling bubble cavitation to a developed cavity is rapid and occurs with a slight lowering of the exit pressure (or cavitation number). The diminutive cavity is very unstable at this stage (high cavitation number) and is occasionally cleared by the approaching liquid flow. As the cavitation number is reduced the cavity grows longer and the frequency

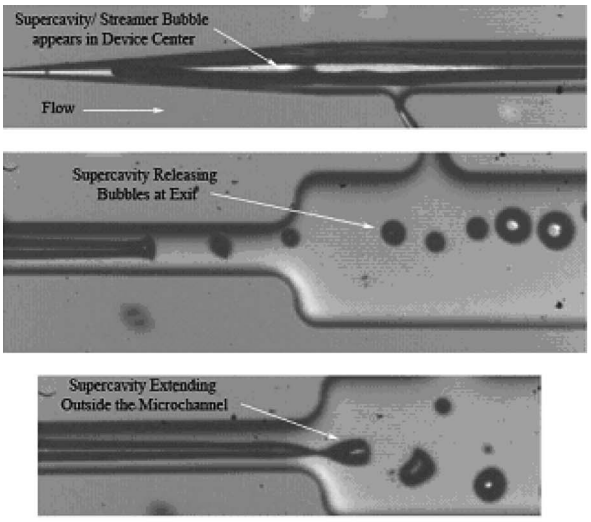

FIG. 2. (a) Appearance of a single streamer bubble/supercavity, which bifurcates the flow and extends to the microchannel exit (σ_V=0.255). (b) Vapor from the developed cavity touching the top Pyrex surface (σ_V =0.724).

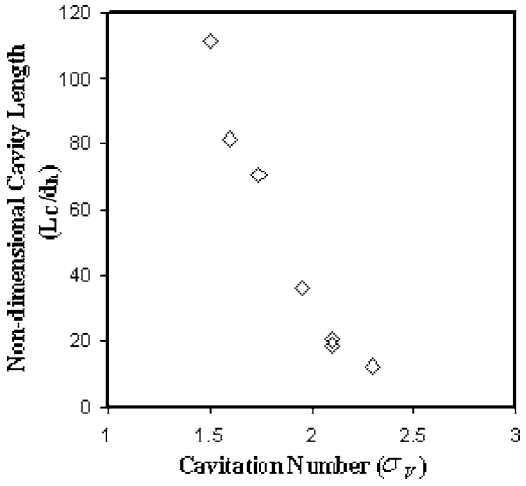

FIG. 3. Variation of cavity length with a reducing cavitation number.

and size of the emitted bubbles ramp up. This is quite expected since a reduction in the cavitation number necessarily means an increase in the intensity of cavitation events. However, on reduction of the exit pressure, the bubbles which are shed from the cavity appear to lose their spherical structure and display an elongated form. The distortion of the bubble shape is suspected to be a direct contribution/confinement effect[18] of the microchannel walls.

Proceeding in a similar vein and reducing the cavitation number merely results in lengthening the long cavity into the microchannel. Upon sufficient reduction of the exit pressure; i.e., the cavitation number, the long cavity stretches and sometimes extends beyond the exit of the microchannel (Fig. 2). The elongated supercavity (streamer bubbles[19,20]) experiences sporadic shedding and large bubbles are observed to be emerging from the cavity near the microchannel exit in the form of a bubble jet. A quantification and variation of the cavity length with the cavitation parameter has been provided in Fig. 3. The end segment of the elongated streamer bubble becomes unstable at times, and large portions of the supercavity are ripped off from the end of the augmented cavity [Fig. 2(a)]. In all previous macroscale experiments on cavitating Venturis, a reduction in the cavitation number simply caused an increase in the cavitation intensity near the Venturi throat and choking of the discharge.[19–21] The supercavity splits the flow and the area available for the liquid is greatly reduced which in turn hastens to increase the local velocity of the liquid near the top and bottom of the cavity. The emergence of local high dynamic heads and concomitant low-pressure conditions assists in maintaining the coherent cavity. This is quite unlike macroscale results for Venturis, where a dense population of cavitation bubbles/twin cavities[17] is formed inside the separation shear layer near the boundaries while a limited number of bubbles are formed in the central liquid core.[21] In the case of micro-orifices, acute cavitation and the presence of twin cavities have been sighted downstream of the constriction element where the contraction and expansion is abrupt.[5,6] The appearance of alternate bright and dark fringes [Fig. 2(b)] near the vapor-liquid interface suggests a curved structure of the vapor cavity. Furthermore, repetition of the aforesaid experiments with a second microdevice possessing a shortened throat (832 μm instead of 1632 μm) resulted in a similar cavitating flow pattern. An appraisal of the available results pertinent to cavitation in high-velocity microfluidic devices[5] and the results obtained for their macroscale counterparts suggests that the formation of a single elongated cavity (streamer bubble or supercavity) in the center of themicrochannel might be a characteristic of cavitation that persists in microhydraulic systems.

B. Venturi discharge coefficient

The micro-Venturi discharge coefficient, which provides an estimate of the losses suffered by the liquid while traversing through the device, is calculated as

$$C_V = \frac{V_{th}}{\sqrt{2(P_1 - P_2) \Big/ \rho\left[1 - \left(\frac{A_{\text{th}}}{A_1}\right)^2\right]}}. \quad (3)$$

The resultant plot of the Venturi discharge coefficient (C_V) shows a monotonous increase with the Reynolds number (increase in the pressure differential) which is not entirely un-

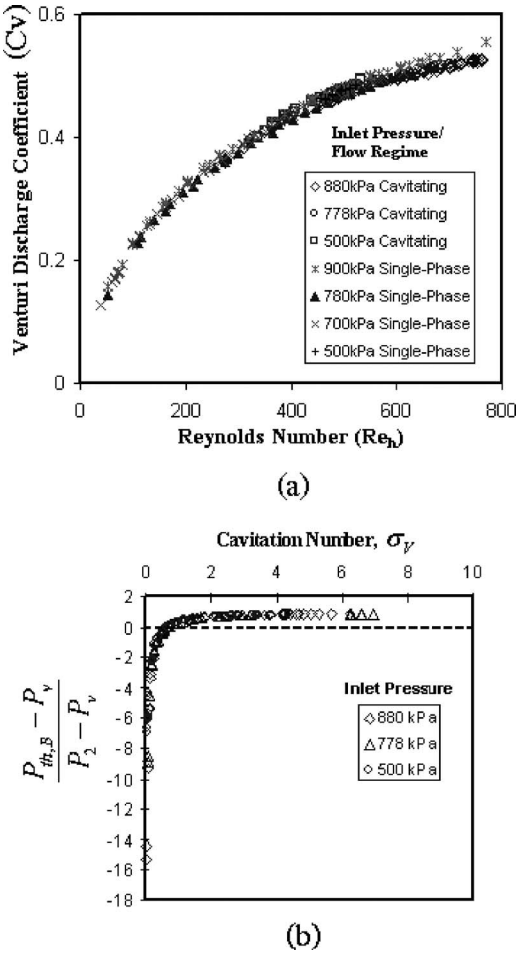

FIG. 4. (a) Micro-Venturi discharge coefficient for both single-phase and cavitating flows. (b) Dimensionless tensile strength plot of the micro-Venturi throat exit pressure at various inlet pressures.

expected [Fig. 4(a)]. In a fully developed flow condition, the viscous losses decrease with increasing Reynolds number, and this is clearly reflected by the increase in the micro-Venturi discharge coefficient. The discharge coefficient (flow rates) obtained for both the cavitating and the single-phase conditions are similar for a particular pressure drop. This is definitely in agreement with the cavitating flow patterns presented. The phenomenon of flow rate choking, which has been reported in several Venturi studies, occurs because of the formation of vapor cavities in the Venturi throat, which is the minimum flow area in the device. However, in the current experiments, cavitation transpires immediately outside the throat of the micro-Venturi, which possesses the minimum flux-averaged flow area. Since the mass flux passes through the area of maximum resistance (or the minimum cross-sectional area of the device), i.e., the Venturi throat, it comes as no surprise that the discharge coefficient does not fall, i.e., no discharge choking, with increase in the pressure differential across the micro-Venturi within the tested range. However, at higher Reynolds numbers (or higher pressure differences) the friction between the two-phases become noticeable and the flow rate diverges (although slightly) from the flow rates achieved during single-phase flow. It is worth mentioning that water has a significantly higher capacity to withstand tension, and a meticulous investigation with a liquid with relative low tensile strength can possibly unveil the choking phenomenon if cavities are noticed at the micro-Venturi minimum cross-sectional area; i.e., the throat.

C. Estimation of throat tensile strength

The minimum pressure in the Venturi system will be felt at the throat exit. Macroscale dynamic-flow experiments by Knapp *et al.*[12] with pressurized water flow through a glass Venturi indicated that untreated water samples (i.e., water containing a large population of nuclei) display no measurable tensile strength due to the availability/significant presence of stream nuclei which trigger cavitation efficiently. The current experiments disclose that cavitation ensues downstream of the throat and the liquid remains mostly unaffected at the throat section, although under a sustained tension. The micro-Venturi throat exit pressure has been estimated based on the exit pressure and a simplified model as a first order approximation which accounts for the losses due to the diffuser section through the expression provided below and presented in Fig. 4(b):

$$P_{\mathrm{th},B} = P_2 - 0.5\rho V_{\mathrm{th}}^2 \left[1 - k_L - \left(\frac{A_{\mathrm{th}}}{A_2} \right)^2 \right], \tag{4}$$

where P_2 is the static pressure downstream of the diffuser section, A_2 is the cross-sectional area of the microchannel/diffuser exit, and $k_L = 0.3$, is the pressure loss coefficient for the small divergence angle diffuser.[22] The profiles of the nondimensional $P_{\mathrm{th},B}$ for different inlet pressures collapse onto a single curve and the $P_{\mathrm{th},B}$ equals the vapor pressure when the curve traverses the x axis. All values below the x-axis show that the liquid present at the Venturi throat is under some tension. The maximum estimated value of the $P_{\mathrm{th},B}$, when cavitation takes place downstream of the Venturi throat, is nearly -152 kPa, which translates into a tension of ~ 150 kPa. It is expected that a working liquid with relative low tensile strength can possibly unveil the choking phenomenon.

V. CONCLUDING REMARKS

The presence of hydrodynamic cavitation in flow of deionized water through micro-Venturis has been identified. Assorted cavitating flow patterns such as traveling bubble cavitation and fully developed streamer bubble/supercavitation have been witnessed and their mechanisms discussed. Incipient cavitation bubbles have been sighted emerging downstream from the micro-Venturi throat, in the bulk of the fluid inside the diffuser and occasionally from the boundaries of the micro device. Under extreme cavitation conditions, the single streamer bubble, which is formed immediately downstream of the micro-Venturi throat, extends into the microchannel. There is no evidence of flow rate choking, as observed in the case of macro-Venturis and the liquid at the minimum flow area withstands high tensions (~ 150 kPa). Cavitation is destined to persist in high-speed microfluidic devices designed with constriction components such as Venturis, if the required hydrodynamic environment, i.e., high velocity and low static pressures, reign.

ACKNOWLEDGEMENTS

This work was partly supported by the National Science Foundation under Contract No. CTS-0520604. Graduate student support from Rensselaer Polytechnic Institute is gratefully acknowledged. The microfabrication was performed at the Cornell NanoScale Facility (a member of the National Nanotechnology Infrastructure Network) which is supported by the National Science Foundation under Grant No. ECS-0335765, its users, Cornell University and industrial affiliates. The authors would like to extend their gratitude to the staff and students of the CNF.

[1] A. H. Epstein and S. D. Senturia, "Macro power from micro machinery," Science **276**, 1211 (1997).
[2] C.-M. Ho and Y.-C. Tai, "Micro-electro-mechanical-systems (MEMS) and fluid flows," Annu. Rev. Fluid Mech. **30**, 579 (1998).
[3] P. Gravesen, J. Branebjerg, and O. S. Jensen, "Microfluidics—a review," J. Micromech. Microeng. **3**, 168 (1993).
[4] H. A. Stone, A. D. Strooch, and A. Ajdari, "Engineering flows in small devices: Microfluidics toward a lab-on-a-chip," Annu. Rev. Fluid Mech. **36**, 381 (2004).
[5] C. Mishra and Y. Peles, "Cavitation in flow through a micro-orifice inside a silicon microchannel," Phys. Fluids **17**, 013601 (2005).
[6] C. Mishra and Y. Peles, "Size scale effects on cavitating flows through micro-orifices entrenched in rectangular microchannels," J. Microelectromech. Syst. **14**, 987 (2005).
[7] C. Mishra and Y. Peles, "Flow visualization of cavitating flows through a rectangular slot micro-orifice ingrained in a microchannel," Phys. Fluids **17**, 113602 (2005).
[8] S. Pennathur, Y. Peles, and A. H. Epstein, "Cavitation at micro-scale in MEMS fluid machinery," in *Proceedings of the ASME International Mechanical Engineering Congress and Exposition*, New Orleans, 2002, Micro-Electromechanical Systems (MEMS) Division Publication (ASME, New York, 2002), p. 87.
[9] L. d'Agostino and A. J. Acosta, "Separation and surface nuclei effects in a cavitation susceptibility meter," J. Fluids Eng. **113**, 695 (1991).
[10] C. E. Brennen, *Cavitation and Bubble Dynamics* (Oxford University Press, Oxford, UK, 1995).
[11] J. W. Holl, "Nuclei and cavitation," J. Basic Eng. **92**, 681 (1970).
[12] R. T. Knapp, J. W. Daily, and F. G. Hammit, *Cavitation* (McGraw-Hill, New York, 1970).
[13] L. d'Agostino and A. J. Acosta, "Cavitation susceptibility meter with optical cavitation monitoring. Part one. Design concepts," J. Fluids Eng. **113**, 261 (1991).
[14] L. d'Agostino and A. J. Acosta, "Cavitation susceptibility meter with optical cavitation monitoring. Part two. Experimental apparatus and results," J. Fluids Eng. **113**, 270 (1991).
[15] S. J. Kline and F. A. McClintock, "Describing uncertainties in single-sample experiments," Mech. Eng. (Am. Soc. Mech. Eng.) **75**, 38 (1953).
[16] K. Sato, K. Hachine, and Y. Saito, "Inception and dynamics of traveling-bubble-type cavitation in a Venturi," in *Proceedings of the 4th ASME/JSME Joint Fluids Engineering Conference*, Honolulu, HI (ASME, New York, 2003), Vol. 2(A), p. 279.
[17] J. H. Gummer and M. T. Thew, "Venturi investigations into cavitation in ethylene glycol/water mixtures," J. Process Mechanical Engineering **212**, 235 (1998).
[18] T. M. Pham, J. M. Michel, and Y. Lecoffre, "Dynamical nuclei measurement: On the development and the performance evaluation of an optimized center-body meter," J. Fluids Eng. **119**, 744 (1997).
[19] Y. Ito and R. Oba, "Cavitation shock pressures in a Venturi," Reports of The Institute of High Speed Mechanics, Tohoku University **37**, 29 (1978).
[20] Y. Ito and R. Oba, "A limited role of separation bubble in desinent cavitation," J. Fluids Eng. **107**, 121 (1985).
[21] T. Ishii and M. Murakami, "Comparison of cavitation flows in He I and He II," Cryogenics **43**, 507 (2003).
[22] V. L. Streeter, *Handbook of Fluid Dynamics* (McGraw-Hill, New York, 1961).